IOP Publishing Superconductor Science and Technology
Supercond. Sci. Technol. **29** (2016) 034005 (8pp) doi:10.1088/0953-2048/29/3/034005

# Trapped magnetic-field properties of prototype for Gd-Ba-Cu-O/$MgB_2$ hybrid-type superconducting bulk magnet

**Tomoyuki Naito[1], Hidehiko Mochizuki[1], Hiroyuki Fujishiro[1] and Hidekazu Teshima[2]**

[1] Faculty of Engineering, Iwate University, Morioka 020-8551, Japan
[2] Nippon Steel & Sumitomo Metal Corporation, Futtsu 293-8511, Japan

E-mail: tnaito@iwate-u.ac.jp

Received 21 October 2015, revised 1 December 2015
Accepted for publication 10 December 2015
Published 25 January 2016

**Abstract**

We have studied experimentally and numerically the trapped magnetic-field properties of a hybrid-type superconducting bulk magnet, which comprised an inner Gd-Ba-Cu-O (GdBCO) disk-bulk and an outer $MgB_2$ ring-bulk, under field-cooled magnetization (FCM) and pulsed-field magnetization (PFM). The trapped field by FCM at the center of the hybrid bulk was 4.5 T at 20 K, which was 0.2 T higher than that of the inner GdBCO disk-bulk without $MgB_2$ ring-bulk. The experimental results by FCM were quantitatively reproduced by the numerical estimations for a model, which makes it possible to understand the trapped field properties of the hybrid bulk. The total magnetic flux by FCM, which was estimated numerically, was enhanced by about 1.7 times from 0.91 mWb of the single GdBCO bulk to 1.53 mWb of the hybrid bulk. We also succeeded in magnetizing the whole hybrid bulk by applying multi-pulsed-fields. The central trapped field of 1.88 T was not enhanced, but the total magnetic flux, which was obtained experimentally, was evidently increased by 2.5 times (0.25 → 0.62 mWb) for the hybrid bulk. The obtained results suggest that the hybridization is effective to enhance the total magnetic flux. To confirm the reinforcing effect of the $MgB_2$ ring to the GdBCO disk during the cooling and magnetization processes, we have measured the thermal dilatation, $dL(T)/L(300\ K)$, of the GdBCO, $MgB_2$ and stainless steel. As a result, the thermal dilatation of $MgB_2$ was smaller than that of GdBCO. $MgB_2$ ring-bulk shows no compression effect to resist the hoop stress of the GdBCO disk-bulk during the FCM process. The reinforcing material such as the stainless steel ring must be set outside the GdBCO disk-bulk.

Keywords: superconducting bulk magnet, hybrid bulk, field-cooled magnetization, pulsed-field magnetization, $MgB_2$, Gd-Ba-Cu-O

(Some figures may appear in colour only in the online journal)

## 1. Introduction

High field magnet is one of the promising applications for high-temperature superconductors. In addition to a solenoid coil wound by superconducting wire or tape, a superconducting bulk as a 'quasi-permanent' magnet is another crucial candidate [1]. The superconducting bulk magnet offers not only a Tesla-class strong magnetic field, $B_T$, but a large magnetic force field, $B_T \cdot (dB_T/dr)$, where, $dB_T/dr$ ($r$ is a radius of bulk) is a magnetic gradient. A total magnetic flux, $\Phi_T$, which is the surface integral of $B_T$, is also an important parameter for the practical applications such as magnetic separation [2], motor [3], wind power generator [4] and so on. For the enhancement of the efficiency of magnetic devices, the magnetic field must reach long distance from the bulk surface. Using the Bean's critical state model [5], $B_T$ is proportional to both the bulk diameter, $d$, and the critical current density, $J_c$. To enhance the $B_T$ value, $d$ and/or $J_c$ must be increased. In this case, the output power of both motor and generator is enhanced through the enhancement of the torque, $\tau$, which is proportional to the $\Phi_T$ value.

Melt-processed single-domain RE-Ba-Cu-O bulk (REBCO; RE denotes rare-earth element) allows a high $J_c$ over $10^5$ A cm$^{-2}$ to flow through inside itself at 77 K, which generates magnetic field, $B_T^{FCM}$, of several Tesla using field-cooled magnetization (FCM) [6, 7]. The higher $B_T^{FCM}$ can be realised at lower temperatures because of the increase in $J_c$. Therefore, a 10 T class bulk magnet can be realised around 40 K using bulks 45–60 mm in diameter and 15 mm in thickness reinforced by a stainless steel ring [8]. Further high $B_T^{FCM}$ over 17 T was obtained for the specially reinforced YBCO [9] and GdBCO [10] bulks below 30 K. It is difficult to fabricate a large single-grain REBCO bulk over 100 mm in diameter due to the difficulty in controlling the crystal growth. Several unique techniques including a multi-seeding [11], an RE compositional gradient [12, 13] technique and a novel infiltration process using $Gd_2BaO_4$ and Ba-Cu-O precursors [14] enable us to grow the large REBCO bulks with 140–150 mm diameter. In addition, a welding of plural bulks possibly offers a large bulk-tile [15]. On the other hand, a large $MgB_2$ bulk magnet over 100 mm diameter can be fabricated more easily, because 'polycrystalline' $MgB_2$ bulks (20–65 mm diameter) are known to trap Tesla-class magnetic field [16–21]. However, their trapped field is smaller than that of the REBCO bulk because of the strong suppression in $J_c$ under magnetic field. $B_T^{FCM} = 5.4$ T at 12 K is the highest trapped field on the $MgB_2$ bulk to date [19].

Pulsed-field magnetization (PFM) is promising to magnetize the superconducting bulks set in the practical applications. However, it is well known that the large temperature rise due to the intense motion of vortices strongly suppresses the trapped field, $B_T^{PFM}$, which is generally lower than that obtained by FCM. A multi-pulsed-fields application, which reduced the vortex motion, realised $B_T^{PFM} = 5.2$ T at 30 K on the GdBCO bulk with 45 mm diameter, which is known to be a record-high value [22]. The smaller $B_T^{PFM} = 3.0$ T at 40 K on the larger GdBCO bulk with 65 mm diameter suggests that the pulsed field up to about 7 T, which is generally determined by a capacitor bank, is insufficient to magnetize the large bulks over 65 mm in diameter [23]. $MgB_2$ bulks, which were fabricated by various techniques, have been magnetized by PFM [24–26]. The $B_T^{PFM}$ of 0.80 T at 14 K on the highly dense $MgB_2$ bulk with 38 mm diameter is the highest value [26]. The flux-jump phenomena prevent the enhancement of the $B_T^{PFM}$ in $MgB_2$ bulk in spite of the abundant magnitude of pulsed fields.

To overcome the weaknesses for each bulk and the magnetization techniques, we propose a hybrid-type bulk magnet in the present study, which consists of the inner REBCO disk-bulk and the outer $MgB_2$ ring-bulk. The hybrid bulk is expected to offer the enhancement of the trapped field and total trapped flux simultaneously due to the enlargement of the bulk diameter. Since the $B_T$ profile on the bulk is conical under full magnetization, a bulk with high $J_c(\mu_0 H)$ must be placed inside and that with low $J_c(\mu_0 H)$ outside in the hybrid bulk, where $\mu_0 H$ is the external magnetic field.

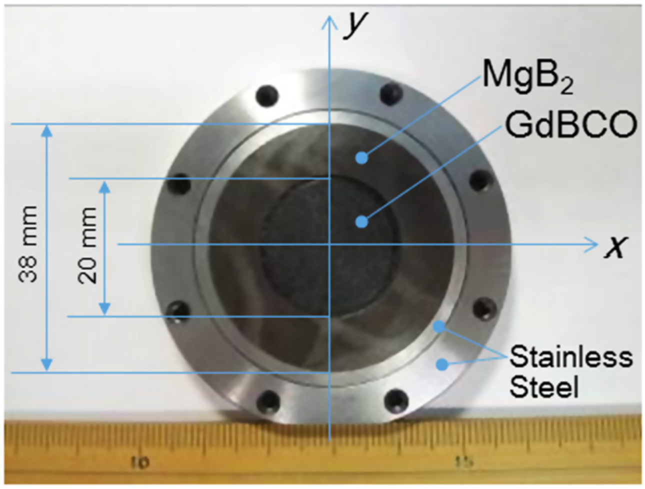


**Figure 1.** Photograph of the hybrid bulk with stainless steel rings. The center circle is the GdBCO disk and the ring is $MgB_2$. The black space between the bulks is the epoxy resin. Two-dimensional orthogonal coordinate axes are defined. The *x*- and *y*-axes are in the plane parallel with the bulk surface and the origin is set at the center of the bulk surface.

The $J_c(\mu_0 H)$ value of the GdBCO bulk was reported to be $\sim 10^5$ A cm$^{-2}$ at 20 K under 3 T [27], which is about two orders of magnitude larger than that of the dense $MgB_2$ bulk under the identical conditions [18]. If one fabricates the hybrid bulk with the opposite configuration, that is, the inner $MgB_2$ disk-bulk and the outer REBCO ring-bulk, the trapped field of the central $MgB_2$ should be fairly reduced by the magnetic field generated by the REBCO ring-bulk. In this sense, this type of hybrid bulk is unrealistic. In this paper, we produce a prototype for the hybrid bulk magnet using the inner GdBCO disk- and outer $MgB_2$ ring-bulks, evaluate its trapped field properties by FCM and PFM experimentally and numerically, and discuss the possibility of producing a hybrid-type bulk magnet. The present hybrid bulk magnet is operated around 20 K taking the mechanical strength of the GdBCO bulk into account, because the bulk is often broken by the hoop stress due to the Lorentz force, $F_L$ [28]. Therefore, we also measured the thermal dilatation of the GdBCO, $MgB_2$ bulks and the stainless steel, to evaluate the possibility of a compression effect of $MgB_2$ ring-bulk on the hoop stress to the GdBCO disk-bulk.

## 2. Experimental procedure

### 2.1. Hybrid bulk preparation

Figure 1 shows a photograph of the hybrid bulk, which consists of the central disk-shaped GdBCO bulk (20 mm in diameter and 7 mm in thickness), the ring-shaped $MgB_2$ bulk (22 mm in inner diameter, 38 mm in outer diameter, and 7 mm in thickness) with outer stainless steel (SS) rings. GdBCO bulk was grown by the modified quench and melt growth (QMG) method [29], which was described in detail elsewhere [8]. As-grown bulk machined into a disk of 20 mm in diameter and 7 mm in thickness was annealed at 673 K for 100 h in flowing 0.1 MPa oxygen gas. $MgB_2$ disk-bulk with 38 mm diameter and 7 mm thickness was fabricated by an *in situ* hot isostatic pressing (HIP) method [18] and was machined by dry process. After the evaluation of the trapped field, the $MgB_2$ disk was drilled into a ring with the inner diameter of 22 mm by a wire electric discharge machine (wet process). The GdBCO and $MgB_2$ bulks and outer SS rings were glued using a thermal conductive epoxy resin STYCAST 2850GT.

### *2.2. Measurements*

The hybrid bulk was magnetized by field cooling (FC) in a static magnetic field of 5 T parallel to the thickness direction at 20 K using a 10-T cryogen-free superconducting magnet (JMTD-10T100, Japan Superconductor Technology (JASTEC), Inc.) and then the applied magnetic field was ramped down to 0 T at a rate of 0.022–0.222 T min$^{-1}$. In PFM, a magnetic pulse up to 6 T with a rise time of 12 ms and a duration time of 150 ms was applied to the zero-field-cooled hybrid bulk at the target temperature. For both FCM and PFM measurements, the bulk was placed on the cold-stage of a Gifford–McMahon-type helium refrigerator by inserting a thin indium sheet to obtain a good thermal contact. The temperature of the cold-stage was controlled with a Pt-Co thermometer and 50 W heater. The trapped field was measured by a transverse-type cryogenic Hall sensor (BHT-921, F.W. Bell Inc.) mounted on the bulk surface using GE7031 varnish in FCM. During PFM, the trapped field at the central bulk surface was measured by a fixed axial-type Hall sensor. The map of the trapped field by PFM was measured at 1 mm above the bulk surface by scanning the Hall sensor using the *x-y* stage. The temperature of the bulk was monitored by a Cernox thermometer which was adhered beside the Hall sensors on the bulk surface in the FCM and was fixed on the SS ring in the PFM.

The thermal dilatation, $dL(T)/L(300\,\mathrm{K})(= (L(T)–L(300\,\mathrm{K}))/L(300\,\mathrm{K}))$, was estimated against for the sample length at 300 K, $L(300\,\mathrm{K})$, using a strain gauge method. A commercial strain gauge (CLFA-350–11, gauge factor = 2.09, Tokyo Sokki Kenkyujo Co., Ltd.) was adhered on the surface of a rectangular-shaped sample with similar superconducting characteristics using an epoxy resin adhesive (EA-2A, Tokyo Sokki Kenkyujo Co., Ltd.). The $dL(T)/L(300\,\mathrm{K})$ of the GdBCO was measured in the *ab*-plane.

### *2.3. Numerical model for simulation*

Trapped field properties of the hybrid bulk were estimated numerically by analyzing the electromagnetic fields using a commercial finite-element-method (FEM) software, Photo-Eddy (PHOTON Co., Ltd., Japan). The simulation was performed at a constant temperature of 20 K, because the experimental temperature rise during the FCM was as small as 0.1 K on the bulk surface. The numerical model with two-dimensional axisymmetric coordinates was developed on the basis of the experimental set-up, which was detailed

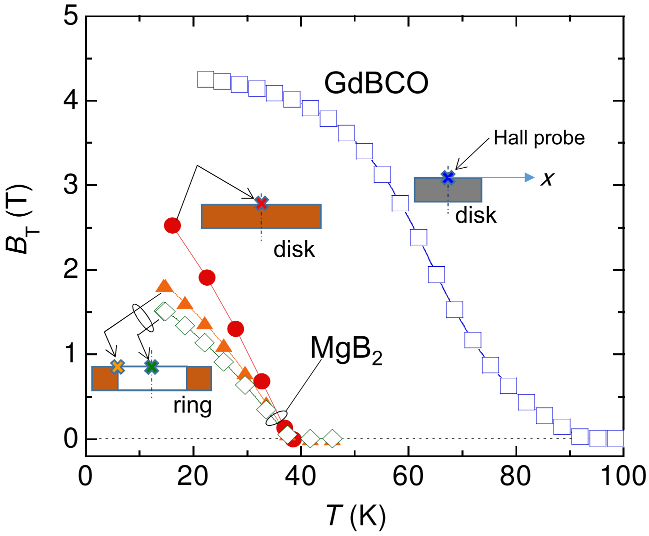


**Figure 2.** Temperature dependence of the trapped field by FCM, $B_T^{FCM}(T)$, for the GdBCO disk- and $MgB_2$ disk- and $MgB_2$ ring-bulks. The bulk and the position of the Hall probe are depicted schematically.

elsewhere [30]. The nonlinear relationship between the electric field, $E$, and the current density, $J$, for each superconductor was described by the power-$n$ model,

$$E = E_c \left( \frac{J}{J_c} \right)^n, \tag{1}$$

where $E_c$ of 1 $\mu$V m$^{-1}$ is an electric-field criterion and $n = 8$ for GdBCO and $n = 100$ for $MgB_2$. The $J_c(\mu_0 H)$ for $\mu_0 H \| c$-axis obtained experimentally for GdBCO bulk was fitted by the following Kim model [31],

$$J_c(\mu_0 H) = \alpha_1 \left\{ 1 - \left( \frac{T}{T_c} \right)^{\frac{1}{2}} \right\}^{\frac{3}{2}} \frac{\mu_0 H_0}{|\mu_0 H| + \mu_0 H_0}. \tag{2}$$

Here, $\alpha_1$ of $2.5 \times 10^6$ A cm$^{-2}$ is the $J_c$ at 0 T and 0 K, $T_c = 94$ K and $\mu_0 H_0 = 5$ T. For the $MgB_2$ bulk, the different $J_c(\mu_0 H)$ fitting function [32] was used as follows,

$$J_c(\mu_0 H) = \alpha_2 \left\{ 1 - \left( \frac{T}{T_c} \right)^2 \right\}^{\frac{3}{2}} \exp\left\{ -\left( \frac{\mu_0 H}{\mu_0 H_0} \right)^\beta \right\}, \tag{3}$$

where the fitting parameters are $\alpha_2 = 4.5 \times 10^5$ A cm$^{-2}$, $\mu_0 H_0 = 1.3$ T, $\beta = 1.7$ and $T_c = 39$ K; $\alpha_2$ is also the $J_c$ at 0 T and 0 K.

## 3. Results and discussion

### *3.1. Field-cooled magnetization (FCM)*

*3.1.1. Trapped field properties of the individual GdBCO and $MgB_2$ bulks by FCM.* Figure 2 shows the temperature dependence of the trapped magnetic field determined by FCM, $B_T^{FCM}(T)$, for the GdBCO disk-bulk, $MgB_2$ disk-bulk and $MgB_2$ ring-bulk. Hereafter, we call the single bulk using

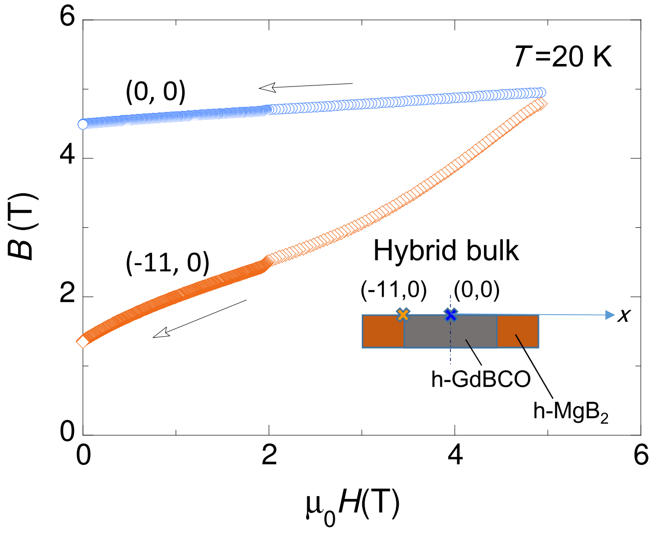


**Figure 3.** Magnetic-field dependence of the magnetic-flux density, $B$, at both the (0, 0) and $(-11, 0)$ positions for the hybrid bulk at $T = 20$ K under the field-cooled magnetization process.

prefix 's-' as with s-GdBCO and s-$MgB_2$. Two-dimensional orthogonal coordinate axes are defined as shown in figure 1. The $x$- and $y$-axes are in the plane of the bulk surface and the origin is set at the center of the hybrid bulk. The position of the Hall probe is schematically shown in figure 2. The s-GdBCO disk-bulk was magnetized from $\mu_0 H = 5$ T at 22 K, and the trapped field of 4.3 T was achieved at the (0, 0) position. Quite a moderate decrease in $B_T^{FCM}(T)$ with elevated temperature was observed from 22 to around 50 K, and subsequently $B_T^{FCM}$ decreases rapidly with increasing temperature above 50 K and finally reaches zero at the critical temperature, $T_c = 94$ K.

On the other hand, the s-$MgB_2$ disk-bulk was magnetized at 14.5 K and the $B_T^{FCM}$ of 2.5 T was obtained at the (0, 0) position. $B_T^{FCM}$ decreases monotonically with increasing temperature, and reaches zero at $T_c = 39$ K. After the s-$MgB_2$ disk-bulk was manufactured as a ring form, the s-$MgB_2$ ring-bulk was magnetized at 16 K. A glass-fibre reinforced plastic (GFRP) disk with 22 mm diameter and 7 mm thickness was inserted into the hollow of the ring, and two Hall probes were set at the bulk center (0, 0) and the edge of the inner circle $(-11, 0)$ positions, respectively. The $B_T^{FCM}$ values at both positions, respectively, are 1.5 T and 1.8 T at 16 K, which come from the fact that the magnetic flux of the ring-shaped bulk tends to concentrate around the inner edge.

#### 3.1.2. *Trapped field properties of hybrid bulk by FCM.*

Figure 3 shows the magnetic-field dependence of the magnetic-flux density, $B$, at both the (0, 0) and $(-11, 0)$ positions for the hybrid bulk under the FCM process at 20 K. The sweep rate of $\mu_0 H$ was changed from $-0.222$ to $-0.022$ T min$^{-1}$ at $\mu_0 H = 2$ T, to avert the quench phenomenon. The $B$ values at each position decrease monotonically with decreasing $\mu_0 H$. We finally obtained the trapped fields, $B_T^{FCM}$, of 4.5 and 1.4 T, respectively, at each position.

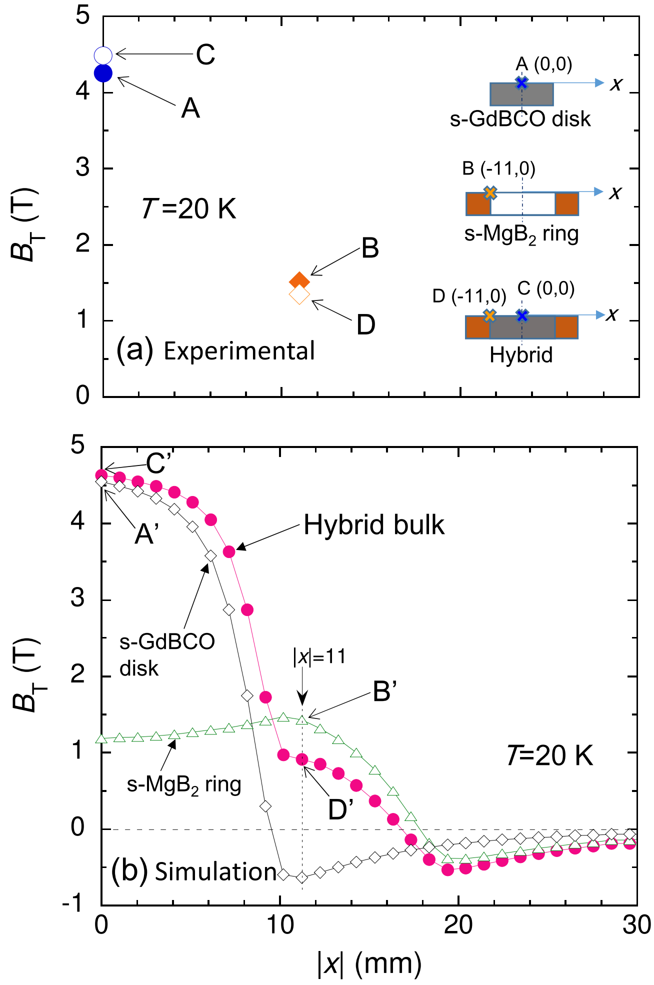


**Figure 4.** (a) Experimentally obtained trapped field by FCM, $B_T^{FCM}$, at the C(0, 0) and D$(-11, 0)$ positions for the hybrid bulk at 20 K. The $B_T^{FCM}$ at the A(0, 0) position for the single GdBCO disk-bulk and at the B$(-11, 0)$ position for the hollow $MgB_2$ ring-bulk are also plotted for comparison. (b) Cross-sections of the trapped field profiles obtained by numerical simulation for various bulks studied here (see text). The simulated plots A', B', C' and D' correspond to the experimental plots A, B, C and D.

Figure 4(a) shows the $B_T^{FCM}$ values of the hybrid bulk at the (0, 0) and $(-11, 0)$ positions at 20 K, which were extracted from figure 3. The $B_T^{FCM}$ values of each single bulk at the identical position are also plotted, which were extracted from figure 2. Hereafter, we call each constitutional part in the hybrid bulk using the prefix 'h-' as with h-GdBCO and h-$MgB_2$. The $B_T^{FCM}$ of 4.5 T at the (0, 0) position of the hybrid bulk (point C) is enhanced by 0.2 T compared to that for the s-GdBCO disk-bulk at the same position (point A). This originates from the superposition of the trapped magnetic fields within the h-GdBCO disk and h-$MgB_2$ ring. However, the magnitude of the $B_T^{FCM}$ increase is rather smaller than that expected from the sum of $B_T^{FCM}$ of each single bulk. In addition, the $B_T^{FCM}$ value at the $(-11, 0)$ position reduces from 1.5 T of the hollow s-$MgB_2$ ring-bulk (point B) to 1.4 T of the hybrid bulk (point D). The

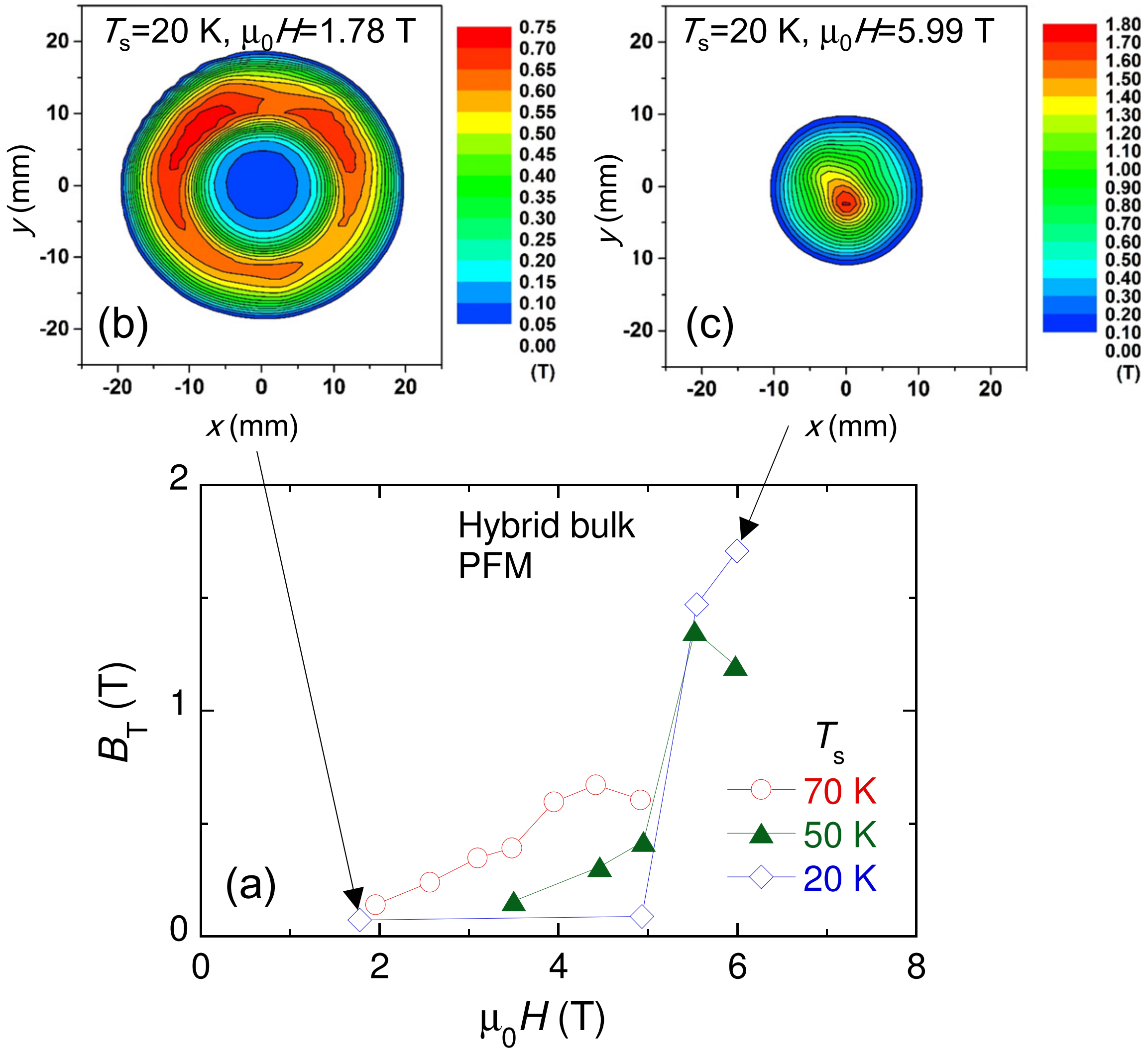


**Figure 5.** (a) Applied pulsed-field dependence of the trapped field, $B_T^{PFM}$, of the hybrid bulk by PFM for various temperatures, $T_s$. The $B_T^{PFM}$ mapping of the hybrid bulk at $T_s = 20$ K for (b)$\mu_0 H = 1.78$ T and (c) 5.99 T.

trapped field surely leaks outside the bulk. This leakage field, $B_{leak}$, along the $z$-axis has an opposite direction compared to the internal $B_T^{FCM}$. Thus, the inverse $B_{leak}$ of the h-GdBCO disk reduces the $B_T^{FCM}$ of the h-$MgB_2$ ring.

The $B_T^{FCM}$ values were obtained experimentally only at $x = 0$ and $-11$ mm. To investigate precisely the experimental results, we simulated the cross-section of the trapped field profile by FCM at 20 K for the hybrid bulk, as shown in figure 4(b). The results of the simulation for the single bulks (s-GdBCO disk and s-$MgB_2$ ring) were also shown. The $B_T^{FCM}$ profile of the hybrid bulk shows the two-step change due to the contribution of each constitutional part. The $B_T^{FCM}$ of the h-GdBCO disk ($|x| = 0 - 10$ mm) enhances entirely as compared with that of the s-GdBCO disk-bulk. The simulated $B_T$-increase at $|x| = 0$ mm from points A′ (4.55 T) to C′ (4.63 T) is about 0.1 T, which is rather small but qualitatively consistent with the experimental one of 0.2 T between points A (4.26 T) and C (4.49 T). On the other hand, a suppression in $B_T^{FCM}$ is found for the entire h-$MgB_2$ ring ($|x| = 11 - 19$ mm) relative to the $B_T^{FCM}$ of the hollow s-$MgB_2$ ring-bulk. The $B_T$-reduction of about 0.5 T at $|x| = 11$ mm from point B′ (1.43 T) to D′ (0.92 T) is somewhat larger than the experimental one of 0.2 T between points B (1.51 T) and D (1.35 T). These discrepancies between the simulated and experimental results come from the slightly large simulated $B_T^{FCM}$ of the h-GdBCO disk compared to the experimental one. In the simulation, the larger $B_{leak}$ due to the larger $B_T^{FCM}$ of the h-GdBCO disk causes the smaller $B_T^{FCM}$ of the h-$MgB_2$ ring, and then results in the small increase of the central $B_T^{FCM}$ by hybridization. In this way, the experimental results are qualitatively reproduced by the numerical simulations.

We compare the total magnetic flux, $\Phi_T$, between the hybrid bulk and the s-GdBCO disk-bulk. The $\Phi_T$ of the hybrid bulk is calculated to be 1.53 mWb from the $B_T^{FCM}$ profile at 20 K, which is 1.7 times lager than that of 0.91 mWb for the s-GdBCO disk-bulk. Therefore, the hybrid configuration is quite effective to enhance $\Phi_T$.

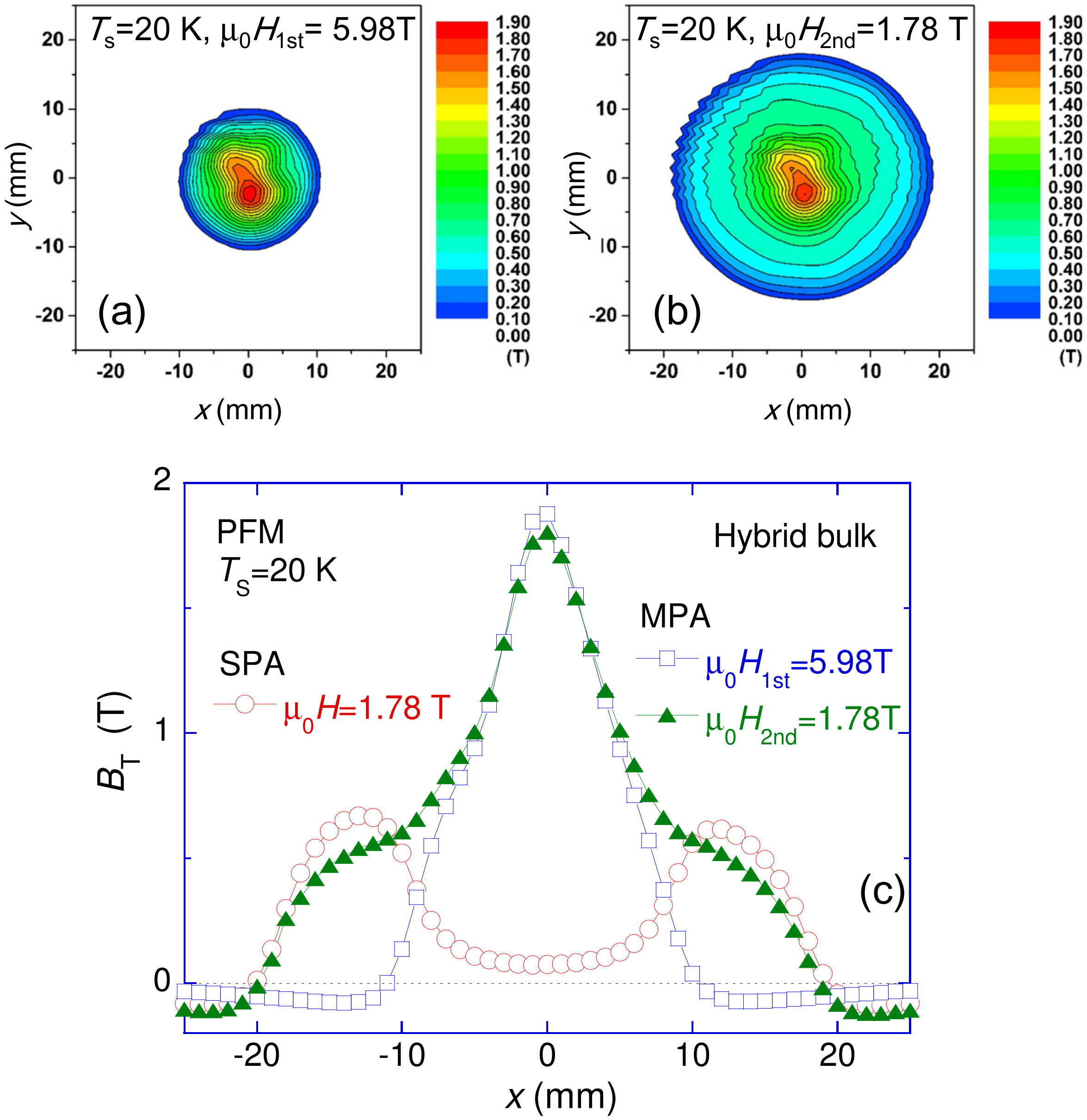


**Figure 6.** The mapping of the trapped field, $B_T^{PFM}$, by the multi-pulsed-fields application (MPA) of the hybrid bulk at 20 K for (a) $\mu_0 H_{1st} = 5.98$ T and (b) $\mu_0 H_{2nd} = 1.78$ T. (c) The cross-section of the $B_T^{PFM}$ profiles at 20 K for SPA of 1.78 T extracted from figure 5(b) and for MPA extracted from figures 6(a) and (b).

### *3.2. Trapped field properties of hybrid bulk by pulsed-field magnetization* (*PFM*)

Figure 5(a) shows the trapped field, $B_T^{PFM}$, at the center of the hybrid bulk in dependence on the applied pulsed field for various temperatures, $T_s$. At $T_s = 70$ K, the $B_T^{PFM}$ increases moderately with increasing applied field, takes a maximum of 0.67 T at $\mu_0 H = 4.42$ T, and subsequently decreases. The steep increase in $B_T^{PFM}$ above $\mu_0 H = 4.95$ T and the $B_T^{PFM}$ peak of 1.36 T at $\mu_0 H = 5.52$ T are observed at $T_s = 50$ K, which originates from the enhancement of $J_c$ by cooling. These results are quite similar to those reported for the single GdBCO bulks [22], because of the non-superconducting h-$MgB_2$ ring at both temperatures. At $T_s = 20$ K, in which both h-GdBCO disk and h-$MgB_2$ ring are superconducting, the $B_T^{PFM}$ is 0.07 T at $\mu_0 H = 1.78$ T, increases suddenly above $\mu_0 H = 4.94$ T, and reaches the highest $B_T^{PFM}$ of 1.71 T at $\mu_0 H = 5.99$ T. Figures 5(b) and (c) show the trapped field maps at $\mu_0 H = 1.78$ and 5.99 T, respectively. For $\mu_0 H = 1.78$ T, the magnetic flux was mainly trapped in the h-$MgB_2$ ring, and was hardly trapped around the center of the h-GdBCO disk. On the other hand, the magnetic flux is mainly trapped in the h-GdBCO disk for $\mu_0 H = 5.99$ T. However, the h-$MgB_2$ ring was not magnetized at all, which possibly originated from the large temperature rise, similar to previous reports [24–26]. To magnetize the whole hybrid bulk, the multi-pulsed-fields application (MPA) which consists of the first field of $\mu_0 H_{1st} = 5.98$ T and the second $\mu_0 H_{2nd} = 1.78$ T was carried out. The $B_T^{PFM}$ profiles in the

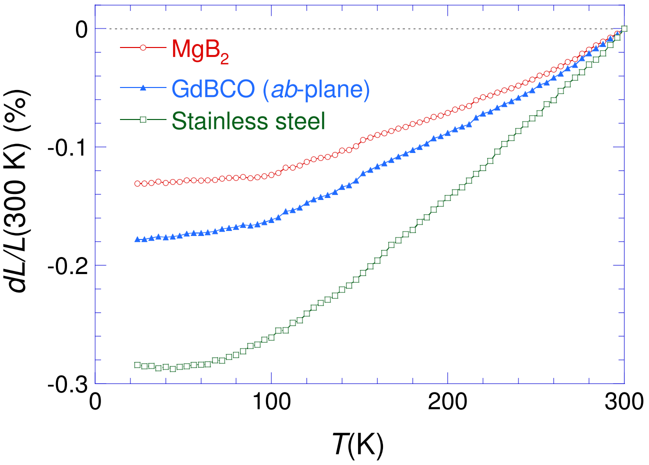


**Figure 7.** Temperature dependence of the thermal dilatation for GdBCO in the *ab*-plane, $MgB_2$ and stainless steel.

*xy*-plane for both stages are shown in figures 6(a) and (b). Similar to the single-pulse application (SPA) of 5.99 T (figure 5(c)), only the h-GdBCO disk is magnetized at $\mu_0 H_{1st} = 5.98$ T. By applying the second pulse, the h-$MgB_2$ ring trapped the magnetic flux. Figure 6(c) shows the cross-section of the $B_T^{PFM}$ profiles of MPA and SPA of 1.78 T at 20 K. The central $B_T^{PFM}$ of 1.88 T at the first pulse was slightly reduced to 1.80 T at the second one, and a similar reduction of $B_T^{PFM}$ is found around the center of the h-GdBCO disk, which is caused by the heat generation due to the vortex motion. The $B_T^{PFM}$ of the h-$MgB_2$ ring by MPA was slightly smaller than that by SPA, which comes from the leakage magnetic field of the h-GdBCO disk. The estimated total magnetic flux, $\Phi_T$, is substantially enhanced from 0.25 mWb for the first pulse application to 0.62 mWb for the second one, which suggests that the hybrid configuration with the MPA technique is quite effective to enhance $\Phi_T$.

### *3.3. Thermal dilatation of each constitutional part of the hybrid bulk*

Finally, let us consider the temperature dependence of the thermal dilatation, $dL(T)/L(300\,\mathrm{K})$, of the constitutional materials such as GdBCO(*ab*-plane), $MgB_2$ and stainless steel (SS), as demonstrated in figure 7. All the materials shrink monotonically with decreasing temperature, and the $dL(T)/L$ (300 K) value is nearly constant below 30 K. The $dL(T)/L$ (300 K) value of $MgB_2$ is smaller than that of both GdBCO bulk and SS, meaning that no reinforcement effect by the h-$MgB_2$ ring on the yield stress of the h-GdBCO disk is expected in the hybrid configuration. Therefore, to achieve higher mechanical strength, we need to insert the SS ring into the space between the h-GdBCO disk- and h-$MgB_2$ ring-bulks. The $dL(T)/L(300\,\mathrm{K})$ value of SS was larger than that of $MgB_2$ bulk, which suggested the reinforcement effect of the SS ring on the $MgB_2$ bulk.

## 4. Summary

We fabricated a prototype of the hybrid bulk magnet consisting of inner GdBCO disk-bulk and outer $MgB_2$ ring-bulk and evaluated its trapped field properties by experiments and numerical simulations. As a result, we could demonstrate the effectiveness of the hybridization from the obtained results as follows.

i. The trapped field of the center of the hybrid bulk was increased by the contribution of the $MgB_2$ ring-bulk by FCM. The maximum trapped field of 4.5 T was achieved at the center of the hybrid bulk by FCM, which was 0.2 T higher than that of the single GdBCO disk-bulk without $MgB_2$ ring-bulk. The trapped field of the $MgB_2$ ring in the hybrid bulk was reduced by the inverse leakage magnetic field of the GdBCO disk, compared with that of the single $MgB_2$ ring-bulk.
ii. Numerical simulations reproduced qualitatively the experimental results of the trapped field properties by FCM, which helped us to understand the magnetizing mechanism of the hybrid bulk. The total magnetic flux calculated numerically increased from 0.91 mWb of the single GdBCO disk-bulk to 1.53 mWb of the hybrid bulk.
iii. The whole hybrid bulk was successfully magnetized by applying the multi-pulsed-fields. Although the trapped field at the central hybrid bulk was about 1.88 T and was not improved by MPA, the total magnetic flux was remarkably increased from 0.25 mWb for the single GdBCO disk-bulk to 0.62 mWb for the hybrid bulk.
iv. The thermal dilatation of the $MgB_2$ bulk was smaller than that of the GdBCO bulk, which suggested that the $MgB_2$ ring did not protect the GdBCO disk from the electromagnetic force and that a reinforcing material such as stainless steel should be inserted into the space between the bulks.

## Acknowledgments

This work was partly supported by JST A-STEP (AS242Z02673L), Hitachi Metals Materials Science Foundation, and JSPS KAKENHI Grant Numbers 23560002, 15K04718, 15K04646.

## References

[1] Gotoh S, Murakami M, Fujimoto H and Koshizuka N 1992 *J. Appl. Phys.* **72** 2404–10
[2] Hayashi H, Tsutsumi K, Saho N, Nishijima N and Asano K 2003 *Physica* C **392–396** 745–8
[3] Matsuzaki H, Kimura Y, Ohtani I, Izumi M, Ida T, Akita Y, Sugimoto H, Miki M and Kitano M 2005 *IEEE Trans. Appl. Supercond.* **15** 2222–5
[4] Ohsaki H, Terao Y and Sekino M 2010 *J. Phys. Conf. Ser.* **234** 032043

[5] Bean C P 1962 *Phys. Rev. Lett.* **8** 250–3
[6] Nariki S, Sakai N and Murakami M 2005 *Supercond. Sci. Technol.* **18** S126–30
[7] Sawh R P, Weinstein R, Carpenter K, Parks D and Davey K 2013 *Supercond. Sci. Technol.* **26** 105014
[8] Teshima H, Morita M, Arayashiki T, Naito T and Fujishiro H 2013 *Phys. Proc.* **45** 61–4
[9] Tomita M and Murakami M 2003 *Nature* **421** 517–20
[10] Durrell J H *et al* 2014 *Supercond. Sci. Technol.* **27** 082001
[11] Sawamura M, Morita M and Hirano H 2003 *Physica* C **392–396** 441–5
[12] Teshima H, Morita M, Okajima N, Terao Y, Sekino M, Ohsaki H and Murakami A 2013 *Proc. of 24th Int. Cryogenic Engineering Conf. (ICEC 24) and Int. Cryogenic Materials Conf. 2012 (ICMC 2012)* ed K Funaki, A Nishimura, Y Kamioka, T Haruyama and H Kumakura (Tokyo: Cryogenics and Superconductivity Society of Japan) pp 879–82
[13] Morita M, Teshima H and Hirano H 2006 *Nippon Steel Technical Report vol 93* Nippon Steel & Sumitomo Metal Corporation pp 18–23
[14] Sakai N, Nariki S, Nagashima K, Miryala M, Murakami M and Hirabayashi I 2007 *Physica* C **460–462** 305–9
[15] Iida K, Yoshioka J, Sakai N and Murakami M 2002 *Physica* C **370** 53–8
[16] Viznichenko R V, Kordyuk A A, Fuchs G, Nenkov K, Müller K H, Prikhna T A and Gawalek W 2003 *Appl. Phys. Lett.* **83** 4360–2
[17] Naito T, Sasaki T and Fujishiro H 2012 *Supercond. Sci. Technol.* **25** 095012
[18] Sasaki T, Naito T and Fujishiro H 2013 *Phys. Proc.* **45** 93–6
[19] Fuchs G, Häßler W, Nenkov K, Scheiter J, Perner O, Handstein A, Kanai T, Schultz L and Holzapfel B 2013 *Supercond. Sci. Technol.* **26** 122002
[20] Yamamoto A, Ishihara A, Tomita M and Kishio K 2014 *Appl. Phys. Lett.* **105** 032601
[21] Naito T, Yoshida T and Fujishiro H 2015 *Supercond. Sci. Technol.* **28** 095009
[22] Fujishiro H, Tateiwa T, Fujiwara A, Oka T and Hayashi H 2006 *Physica* C **445–448** 334–8
[23] Fujishiro H, Tateiwa T, Kakehata K, Hiyama T, Naito T and Yanagi Y 2008 *Physica* C **468** 1477–80
[24] Fujishiro H, Tamura T, Arayashiki T, Oyama M, Sasaki T, Naito T, Giunchi G and Albisetti A F 2012 *Japan. J. Appl. Phys.* **51** 103005
[25] Fujishiro H, Ujiie T, Naito T, Albisetti A F and Giunchi G 2014 *J. Phys. Conf. Ser.* **507** 032016
[26] Fujishiro H, Ujiie T, Mochizuki H, Yoshida T and Naito T 2015 *IEEE Trans. Appl. Supercond.* **25** 1–4
[27] Kii T *et al* 2012 *IEEE Trans. Appl. Supercond.* **22** 4100904
[28] Miyamoto T, Katagiri J, Nagashima K and Murakami M 1999 *Advances in Superconductivity XI* ed N Koshizuka and S Tajima (Tokyo: Springer) pp 725–8
[29] Morita M, Sawamura M, Takebayashi S, Kimura K, Teshima H, Tanaka M, Miyamoto K and Hashimoto M 1994 *Physica* C **235–240** 209–12
[30] Fujishiro H, Naito T and Yoshida T 2014 *Supercond. Sci. Technol.* **27** 065019
[31] Kim Y B, Hempstead C F and Strnad A R 1965 *Phys. Rev.* **139** A1163–72
[32] Xiang F X, Wang X L, Xun X, De Silva K S B, Wang Y X and Dou S X 2013 *Appl. Phys. Lett.* **102** 152601